Journal of
Polymer & Composites

ISSN: 2321-2810 (Online)
ISSN: 2321-8525 (Print)
Volume 13, Regular Issue 2, 2025
DOI (Journal): 10.37591/JoPC

https://journals.stmjournals.com/jopc

Research JoPC

Optimization of Mechanical Properties of 500/7 Grade Ductile Cast Iron (DCI) By Using Smaw: Applications in Reinforced Composites and Thermoplastics Through Taguchi & Gra

Aamir R. Sayed[1,]*, Devesh Kumar[1]

Abstract

Welding, a critical manufacturing process, is broadly engaged to join metals and thermoplastics using heat, pressure, or both. This study inspects the Shielded Metal Arc Welding (SMAW) method to optimize welding parameters and improve the mechanical properties of Ductile Cast Iron (DCI) grade 500/7, a material widely used in high-strength and thermal conductivity applications in aerospace and automotive sectors. Using an L9 OA (orthogonal array), experiments were conducted on nine plates welded with A-1600 electrodes under varying input parameters: current (100, 110, 120 A), preheat temperature (250, 300, 350°C), and interpass temperature (100, 200, 300°C). The mechanical properties—hardness, tensile strength, and impact resistance—were evaluated through destructive testing (DT), while non-destructive testing (NDT) methods included Dye Penetration Testing (DPT), Magnetic Particle Testing (MPT), Radiographic Testing (RT), and visual inspection. The Investigation was performed using the Taguchi-(Grey Relational Analysis) GRA optimization method. Results revealed that electrode A-1600 provided superior performance, with current identified as the most significant factor. Optimal welding parameters—achieved in Experiment 4—embraced a current of 110 A, a preheat temperature of 250°C, and an interpass temperature of 200°C.The findings offer valuable understandings into improving material performance for reinforced composites and thermoplastics, highlighting the significance of parameter optimization in high-performance engineering applications.

Keywords: Mechanical properties, reinforced composites and thermoplastics, high-strength applications, welding optimization, Taguchi method, grey relational analysis

INTRODUCTION

Welding is a process that joins materials by melting and fusing them together. Various techniques like Shielded Metal Arc Welding (SMAW), Gas Metal Arc Welding (GMAW), Gas Tungsten Arc Welding (GTAW), and Flux-Cored Arc Welding (FCAW) are widely used in different industries. Welding is crucial in fields like construction and manufacturing, where strong material bonds are needed. SMAW, or stick welding, is a popular method that creates an electric arc between a flux-coated electrode and the base material, causing both to melt. The flux protects and cools the weld area. Ductile Cast Iron (DCI) is known for its strength, toughness, and ductility, making it perfect for applications requiring materials that can deform without breaking. It is commonly used in automotive components like engine blocks, suspension parts, and in machinery, construction, and agriculture due to its wear resistance and

***Author for Correspondence**
Aamir R. Sayed

[1]Research Scholar, Mechanical Engineering, Poornima University, Jaipur, Rajasthan, India
[1]Faculty of Engineering & Technology, Poornima University, Jaipur, Rajasthan, India

Received Date: December 24, 2024
Accepted Date: February 06, 2025
Published Date: February 25, 2025

Citation: Aamir R. Sayed, Devesh Kumar. Optimization Of Mechanical Properties Of 500/7 Grade Ductile Cast Iron (DCI) By Using SMAW: Applications in Reinforced Composites and Thermoplastics Through Taguchi & GRA. Journal of Polymer & Composites. 2025; 13(2): S204–S222p.

machinability. DCI pipes are also favored for water supply and sewage systems because of their corrosion resistance. Optimization techniques such as the Taguchi Method and Grey Relational Analysis (GRA) are used in welding to improve mechanical properties. The application of such techniques in welding optimization enables the enhancement of mechanical properties, especially in reinforced composites and thermoplastics, for high-performance engineering applications.

An investigation was conducted on SMAW welding for API 5L Grade B PSL 2 pipe using different repair welding techniques. Macro- and microstructural analyses showed consistent macrostructure across samples but differences in microstructure, specifically in ferrite and pearlite phases. Hardness distribution met API 1104 standards, with repair weld 7R showing the highest hardness. Tensile strength met API 5L requirements, with repair weld 5R exhibiting the highest strength.[1]. Various root pass removal methods, including back grinding and back gouging, were applied to SMAW-welded mild steel joints using ASTM A516 Grade 70. Microstructural analysis indicated coarser grains in the back-gouged joints, which affected mechanical properties. Tensile testing demonstrated superior performance in the back-ground joints, underscoring the importance of welding parameters for achieving optimal results [2]. The effects of shielded metal arc welding on nodular cast iron were studied using Eni-CL electrodes. Microstructure, hardness, and tensile strength were evaluated. Metallographic analysis showed phase changes, with the heat-affected zone displaying the highest hardness. Post-welding tensile strength was reduced, highlighting the impact of welding on material properties [3]. The tensile strength of SMAW-welded dissimilar joints between mild steel (MS) and medium carbon steel (CS) was evaluated. Using the Taguchi L9 orthogonal array, optimal welding parameters—Welding Current, Electrode Angle, and Root Face—were identified to maximize tensile strength. Results indicated that Electrode Angle had the greatest influence (73.97%), followed by Root Face (6.24%) and Welding Current (5.12%) [4]. Two Inconel 617 alloy weld joints, created using GTAW and SMAW processes, showed Mo and Cr segregation with secondary phase formation. Microstructural analysis revealed significant dilution at the interface due to similar melting points. Tensile testing at both room and elevated temperatures, along with Charpy impact tests, indicated that GTAW-welded joints exhibited superior mechanical properties, favoring their use in service applications [5]. A dissimilar joint between Inconel 718 and 304L SS was welded using GTAW and SMAW with Ni-based filler materials. Metallographic examination identified an unmixed zone on the 304L side, along with a fully austenitic microstructure and carbide phases within the weld metal. Tensile tests at room temperature indicated failure within the weld metal [6]. This study examines how shielded metal arc welding (SMAW) parameters influence the mechanical properties and angular distortion in SA 516 Grade 70 welded joints. Using the Taguchi method and Grey relational analysis, parameters such as root gap, groove angle, electrode diameter, and preheat temperature were optimized. Nine experimental trials were performed, resulting in enhanced responses. Confirmatory tests validated the optimal settings, which are significant for manufacturing storage tanks, boilers, and pressure vessels [7]. An experimental study explored the relationship between welding parameters—specifically electrode distance, welding speed, and gas flow rate—and weld bead geometry. Torch voltage and welding current were kept constant throughout. Taguchi methods were used across 12 experiments on samples sized 400x200x16mm to optimize the process settings. Optimal parameters were identified as a welding speed of 40 cm/min, a gas flow rate of 18 l/min, and an electrode distance of 45 mm, achieving the best outcomes [8].

This study developed a mathematical model and algorithm to control output parameters, observing a direct relationship between increased welding current and expanded bead geometry [9]. Experiments on Gas Tungsten Arc Welding (GTAW) for AISI 304 and AISI 201 stainless steel helped refine optimal welding conditions. Parameters included a welding current of 75 amps, pure argon gas with up to 8% nitrogen, and a welding speed range of 2-3.5 mm/s. The best results were achieved with 1% nitrogen in argon and a welding speed of 3 mm/s [10]. The study examines 11 welding processes for crack repair in Nodular Cast Iron (NCI) engine blocks, using DEA and TOPSIS methods for evaluation. SMAW is identified as the most effective, followed by furnace welding, GTAW, and PAW, all using high-nickel content electrodes (50-60%). OAW is found to have lower input utilization compared to the other techniques [11]. The author investigated welding of grey cast iron using a Nickel-based electrode through Shielded Metal Arc Welding (SMAW). The study specifically examined the impact of post-weld heat treatment (PWHT) on the material's hardness and microstructure. PWHT was performed at 870°C for 60 minutes to assess changes in the properties of the parent metal zone (PMZ). Results demonstrated that this heat treatment significantly reduced hardness in the PMZ, indicating effective modification of the welded joint. The hardness reduction suggests that PWHT achieved full annealing of the weld, promoting structural homogenization and relieving residual stresses induced during welding. Observing these effects on the microstructure further confirms the process's suitability for grey cast iron, as the optimized PWHT parameters support the weld's durability and performance. This study provides valuable insights into the use of Nickel-based electrodes for welding grey cast iron, highlighting PWHT's critical role in enhancing joint quality and mechanical properties [12]. The author investigated corrosion resistance in surface repair of grey cast iron for pump applications, using SMAW welding with three electrode types: carbon steel (E7018), hardfacing (EN14700), and Nickel-based (ENi-CI). Testing included abrasion resistance via pin-on-disk trials and corrosion testing in a 3.5% NaCl solution. Among the electrodes, the Nickel-based type delivered the best results due to the absence of excessive carbide and martensitic phases, which contributed to improved corrosion resistance and durability. This study highlights the effectiveness of Nickel-based electrodes in enhancing the performance of grey cast iron repairs in corrosive environments [13]. The study examines the welding of ferritic ductile cast iron using SMAW with E7018 and ENi-CI electrodes. Eight 150x75x20mm samples with a V-groove design were tested under different conditions. For E7018 electrodes, preheating at 320°C for 2 hours was necessary, while ENi-CI electrodes required no preheating. Preheating was found to be crucial, and buttering emerged as the most effective technique for welding. Analyses included optical microscopy (OM), scanning electron microscopy (SEM), and mechanical testing for tensile strength, impact resistance, and hardness, providing insights into the weld quality and performance under each condition [14]. The author investigates how high-speed solidification affects the microstructure and microhardness of hypoeutectic grey cast iron (250 HGCI). Cooling methods utilized nitrogen and helium atmospheres, with both conventional and rapid cooling achieved through high-vacuum drop techniques. Analyses using Vickers hardness testing, SEM, and XRD revealed distinct microstructural variations and increased microhardness with faster cooling rates. However, precise individual mapping of these microstructural changes proved challenging. This study highlights the role of cooling rates in enhancing microhardness and provides insight into optimizing microstructure in hypoeutectic grey cast iron through controlled solidification methods [15]. The study explores the MIG welding of dissimilar metals, specifically AISI 409 ferritic stainless steel and AISI 316L austenitic stainless steel, using a butt joint configuration on specimens measuring 60x100x3 mm. The Taguchi L9 array method was applied to optimize welding parameters: welding current (WC) at 100, 112, and 124A, gas flow rate (GFR) at 10, 15, and 20 lpm, and nozzle-to-plate distance (NPD) at 9, 12, and 15 mm. Optimal results were achieved with a welding current of 112A, a nozzle-to-plate distance of 15 mm, and a gas flow rate of 15 lpm, ensuring quality welds [16].

The study employed Gas Metal Arc Welding (GMAW) to weld stainless steel grade SS304, focusing on the effects of varying heat inputs—low, medium, and high—achieved by adjusting the welding current, voltage, and speed. Results indicated that lower heat input produced the best outcomes, enhancing tensile strength, hardness, and microstructural quality. This suggests that carefully controlled, lower heat input can significantly improve the weld properties of SS304, leading to a more resilient and structurally sound joint. The findings underscore the importance of optimized heat management in achieving high-quality welds in stainless steel [17]. The study analyzed the welding of ductile cast iron (DCI), focusing on mechanical properties with varying preheat temperatures from 200°C to 400°C. It was found that avoiding preheat temperatures between 200°C and 300°C is essential, as this range promotes martensite formation in the heat-affected zone (HAZ) and reduces fusion size, both of which negatively impact mechanical properties. For optimal mechanical performance, higher preheat temperatures closer to 400°C were preferred, minimizing brittle phases and enhancing weld quality. This research emphasizes the importance of precise temperature control to improve the

ISSN: 2321-2810 (Online), ISSN: 2321-8525 (Print)

durability and structural integrity of DCI welds [18]. The study focused on pearlitic ductile cast iron (DCI), evaluating mechanical properties and conducting non-destructive testing using five different electrode types and varying preheating conditions. Optimal results were achieved with a preheat temperature of 300°C, enhancing weld integrity. Additionally, stainless steel plates were welded using Shielded Metal Arc Welding (SMAW) to maximize penetration depth. Key welding parameters included current, torch angle, and polarity, which were carefully controlled to optimize weld quality. This investigation highlights the combined effects of electrode choice and preheat in DCI welding and the influence of welding parameters on stainless steel penetration depth [19]. Mild steel (MS) and stainless steel (SS 304) plates were joined using Manual Metal Arc (MMA) welding, applying the Taguchi L9 Array design of experiments (DOE) method. Input variables included root gap, welding speed, current, and electrode angle, with weld strength and deposition rate as output measures. The optimal welding conditions were identified as a 1mm root gap, an electrode angle of 30°, a current of 80 amperes, and a welding speed of 8 mm/s^2. These parameters yielded the best combination of strength and deposition rate, providing guidelines for improved weld quality in MS and SS 304 joints [20]. Stainless steel 409 plates were welded using Gas Metal Arc (GMA) welding, with the Taguchi L9 array applied to determine optimal conditions. An ANOVA analysis was conducted to rank the influence of key parameters. The input parameters included nozzle-to-plate distance (NPD), welding current, and gas flow rate (GFR), while the output parameters measured were ultimate tensile strength (UTS) and percentage elongation (PE). This approach enabled the identification of welding settings that maximize UTS and PE, providing insights into parameter optimization for enhanced weld quality in SS 409 plates [21]. SMAW and GMAW welding techniques were used to join C-45 material, with the objective of evaluating its weldability based on established process standards set by AWS and ASME. The study aimed to assess the material's performance under these welding methods, ensuring compliance with recognized industry guidelines. By examining the welding characteristics and comparing results against these standards, the research provided valuable insights into the suitability of C-45 for welding applications, helping to ensure quality and consistency in the welded joints according to professional welding criteria [22]. Weld quality is influenced by mechanical properties, welding processes, and input parameters. This study optimizes Shielded Metal Arc Welding (SMAW) parameters for ASTM A572 Grade 50 steel joints using the Taguchi L16 array. The results revealed that groove angle significantly affects tensile strength, electrode diameter influences impact strength, and welding current plays a key role in hardness and distortion. These findings led to considerable improvements in the weld's mechanical performance and dimensional accuracy. The study emphasizes the importance of parameter optimization in achieving high-quality welded joints with enhanced strength and reduced defects [23].

The study investigates the influence of process parameters on EN 10120 steel plates (60x30x2.5mm) using the GMAW process. A total of 27 experiments were conducted with a 1mm diameter SG2 electrode. Input parameters included voltage (22, 24, 26 volts), welding speed (WS) (40, 60, 80 cm/min), and current (95, 105, 115 amperes), with macrostructure and depth of penetration (DoP) as the key outputs. The results revealed that current was the most influential parameter on DoP, having approximately 2.5 times the effect of voltage and WS. The optimal conditions for maximum DoP were a welding speed of 80 cm/min, 24 volts, and 105 amperes of current [24]. The author presented a study on the process parameters of GMAW for welding MS plates (100x50x6mm). A 1.2mm diameter copper-coated electrode was used for butt joint welding, with CO2 shielding gas to achieve high-quality welds in terms of mechanical properties, HAZ, and weld bead geometry (BH, BW, DoP, AoP). The input variables included voltage (24, 28, 32V), gas flow rate (GFR) (10, 14, 18 L/min), wire feed rate (WFR) (4.5, 7, 9.5 m/min), and travel speed (TS) (160, 190, 220 mm/min), with a constant DCEP, current of 150-250A, and inclined torch position. The Box-Behnken design, analyzed through RSM and ANOVA, identified WFR as the most influential parameter, followed by voltage and TS. GFR had the least effect. Confirmation tests validated the results, with errors under 2% [25]. The author explored TIG welding of titanium Ti-6Al-4V material (100x24x6mm, cruciform shape) to enhance welding strength using the Taguchi L16 orthogonal array method. The welding process involved two cross plates and one main plate, using an ERTi5 thorium electrode. Input parameters included voltage (10, 14, 18V), current (80, 100, 120A), and welding speed (60, 70, 80 mm/min), with ultimate tensile strength as the output parameter. Tensile tests were performed using a 25 kN load, and ANOVA and S/N ratio were applied to identify optimal process parameters. The results showed that current and voltage significantly affected tensile strength, while welding speed had minimal impact [26]. The author conducted an experiment on IS 2062 steel plates (200x150x20mm) using a 1.2mm diameter 317L SS flux-cored wire. The shielding gas was 95% Ar and 5% CO2 at 16L/min flow rate with a 90° work angle and DCEP polarity. The study optimized FCAW process variables, including nozzle-to-plate distance (NPD) (15-25mm), welding speed (WS) (26-42 cm/min), and welding current (WC) (176-244A) to assess weld geometry, including penetration, bead width, reinforcement, and shape coefficients. Twenty experiments were conducted following RSM, with confirmation tests validating results. Current and NPD were the most influential parameters, while welding speed had minimal impact. The optimal parameters for bead geometry were NPD 17.93mm, current 192.5A, and welding speed 26.35 cm/min [27]. The author conducted TIG welding experiments on Duplex SS2205 material to optimize parameters for maximum tensile strength, using the Taguchi L9 array, Grey Relational Analysis (GRA), Artificial Neural Networks (ANN), and ANOVA. Specimens (200x50x3mm) were welded with ER316L electrode. Process variables included electrode diameter (2, 2.4, 3mm), oxide flux (SiO2, TiO2, and a mixture), shielding gas (pure Ar, Ar with 2-5% H2, and Ar-He mixtures), fusion time (100, 130, 160 sec), and current (150, 200, 250A). Output parameters were depth, ultimate tensile strength (UTS), and hardness. The results demonstrated that combining ANN and Taguchi methods effectively optimized the welding process, with minimal errors and significant improvements [28].

A study investigates the mechanical properties and parametric optimization of Ductile Cast Iron (DCI) 500/7 grade material using an L9 Orthogonal Array (OA) Design of Experiments (DoE) approach with the Taguchi-Grey Relational Analysis (GRA) technique for . Focusing primarily on DCI 500/7 grade, the study's findings have promising applications in composites & thermoplastics welding, which are extensively used in aerospace and automotive components with its high strength application. Shielded Metal Arc Welding (SMAW) was used to join plates with 1600 electrodes. Three key input parameters—current, preheat temperature, and interpass temperature—were tested at three different levels, resulting in nine welded plates for Destructive Testing (DT) and Non-Destructive Testing (NDT).This study proposes optimal process parameters that save time and cost with better mechanical properties.

MATERIAL & METHOD

The experiment consumed the Shielded Metal Arc Welding (SMAW) process on Ductile Cast Iron (DCI) 500/7 grade material with dimensions of 150 mm x 150 mm x 12 mm. The plates, produced at Trufirm Pvt. Ltd., Nagpur, adapted to ASTM, AWS, and other DCI 500/7 standards. Welding was performed using a Diffusion DW 500 MAG machine, operating on a 3-phase supply with a current range of 54-525 amperes. The groove angle was set to 30° per side, forming a 60° total angle with a 1.25 mm root gap. After welding, plates measured 300 mm x 300 mm x 12 mm. An L9 Orthogonal Array (OA) tested three parameters at three levels, resulting in nine welded plates. These were subjected to destructive and non-destructive tests, with comprehensive specifications and process visuals provided. The Figure 1 expresses the complete detail specification of weld plate before welding.

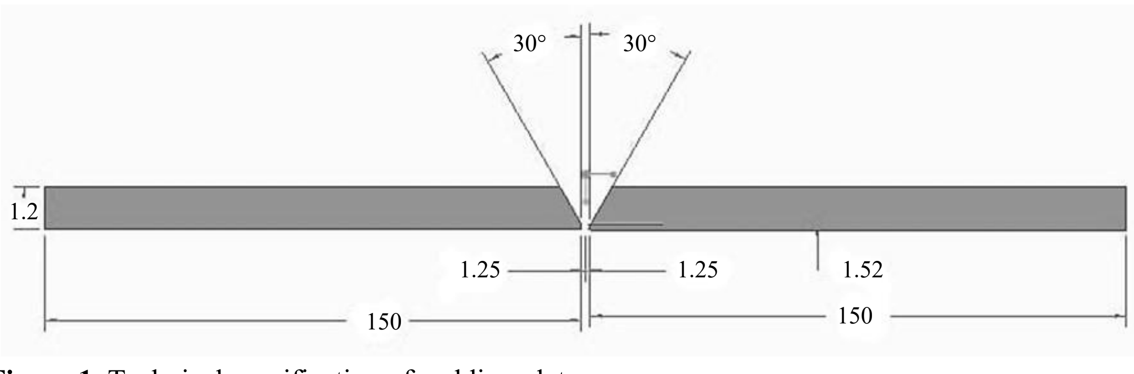

Figure 1. Technical specification of welding plate.

Table 1. Chemical Composition of Base Metal (BM) & A Electrode -1600.

Nam	C	Si	Mn	P	S	Cr	Fe	Mo	V	Cu	W	Co	Nb	Al	Ti	Zr	Sn	B	Pb	Mg	Ta	N	Ni
BM	3.652	2.414	0.461	0.057	0.013	<0.030	92.819	-----	-----	0.413	----	-----	----	----	---	----	----	------	----	0.050	-----	------	<0.020
1600	1.59	0.994	0.729	0.0063	0.00602	<0.0002	34.23	0.00604	0.007	0.102	<0.0003	0.0172	0.00602	0.0705	0.149	***	***	<0.0001	<0.0002	***	***	0.0101	62.1

In the SMAW process, numerous input parameters must be reflected, including the chemical composition of both the material and electrodes, type of welded joint (e.g., butt joint, lap joint, corner joint, T-joint), sample size and material thickness, root thickness and root clearance, electrode types with particular diameters and baking times, welding positions (e.g., 1F, 2F, 3F, 2G, 3G), polarity (DCEP, DCEN), current (amperes), voltage (volts), travel speed (mm/min), number of runs (e.g., root run, 1st run, 2nd run), welding time, preheating temperature, interpass temperature, post-weld temperature, cooling method, and insulation type during cooling [1-12].Based on literature reviews, expert industry advice, and standards from electrode and welding machine manufacturers, three input parameters were selected: current (100–120 amperes), preheat temperature (250°C–350°C), and interpass temperature (100°C–300°C), within the specified ranges. Table 01 provides the chemical composition of the base metal (BM), electrode A-1600.

DESIGN OF EXPERIMENTS AND EXPERIMENTATIONS

The Taguchi L9 Orthogonal Array (OA) was utilized in a Design of Experiments (DoE) to optimize input parameters—current (100-120 A), preheat temperature (250-350°C), and interpass temperature (100-300°C)—and output parameters, including tensile strength, hardness, and impact resistance. Welding was performed with A-1600 electrodes baked at 100°C for 15 minutes. Current, preheat, and interpass temperatures were manually controlled, with a thermal gun ensuring accurate measurements. A specialized fixture stabilized the setup. Root and subsequent weld runs used straight or weaving techniques. Nine plates were welded based on L9 OA combinations, with setup visuals and results outlined in detailed tables. The Table 2 tells the different levels with their input parameters. Table 3 states the design of experiment as per L9 OA for performing the experimentations.

Figure 2 presents images of the welding machine DW 500 displaying current as input parameter, preheat temperature at settings at 100°C, Interpass temperature at 250°C. Figure 3 contains images of the actual welding setup, the root run weld, and the final welded plate after maintaining the input parameters.

Table 2. Levels Of Input Parameters for Experimentation.

	A	**B**	**C**
Levels	***Current (Amp)***	***Preheat temp (°C)***	***Interpass temp (°C)***
1	100	250	100
2	110	300	200
3	120	350	300

Table 3. Design Of Experiments (DoE) For Experimentation as L9 Orthogonal Arrays (OA).

A	B	C
Current (Amp)	***Preheat Temp (^oC)***	***Interpass Temp (^oC)***
1 (100)	1 (250)	1 (100)
1 (100)	2(300)	2 (200)
1 (100)	3(350)	3 (300)
2 (110)	1 (250)	2 (200)
2 (110)	2 (300)	3 (300)
2 (110)	3 (350)	1 (100)
3 (120)	1 (250)	3 (300)
3 (120)	2 (300)	1(100)
3 (120)	3 (350)	2 (200)

Figure 2. Images of input parameters with different input variables.


Figure 3. Images of actual welding setup with root gap and final welded plate.

TESTING OF WELDED PLATE

Destructive Testing (DT), including tensile, hardness, and impact tests, was performed on nine welded plates (300 x 300 x 12 mm), sectioned per ASME/ASTM standards. Non-Destructive Testing (NDT) methods like MPI, DPT, RT, and visual inspection were also applied. Tensile testing used a Universal Testing Machine, hardness testing a hardness tester, and impact testing a Charpy machine. Figure 4 gives the details of one welded plate cut into different testing sections as per the ASME norms. The Figure 5 gives the images of tensile testing, hardness testing and impact testing i.e destructive testing.

Figure 6 and Figure 7 represents the non-destructive testing like RT, MPI , DPT and visual inspection on welded plates.

ISSN: 2321-2810 (Online), ISSN: 2321-8525 (Print)

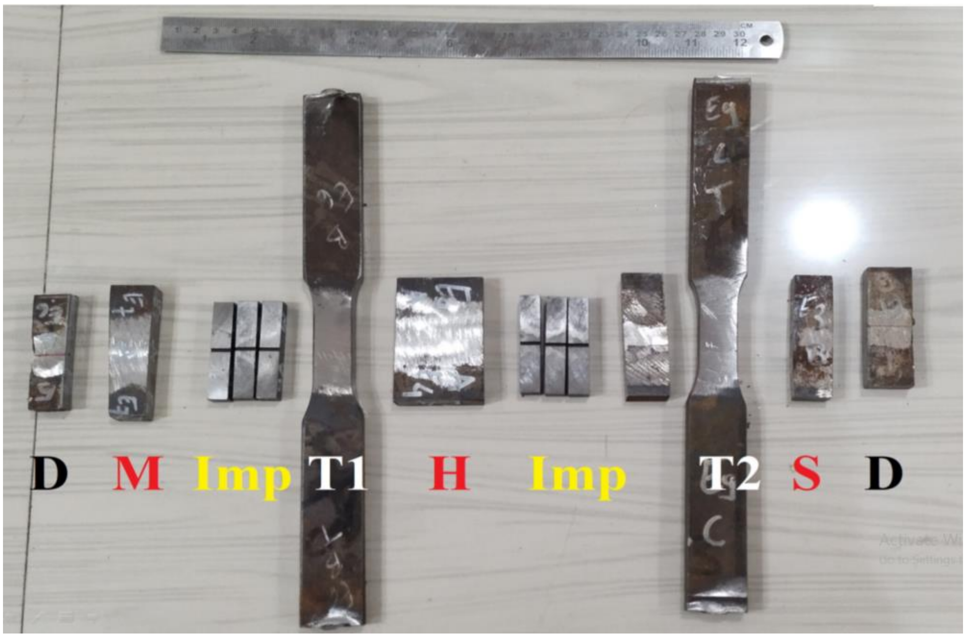

Figure 4. 300 * 300 *12 Mm welded plate cut into different testing samples

Figure 5. Tensile testing, hardness testing & impact testing of 9 welded plate


Figure 6. MPI & DPT of 9 welded plate

Figure 7. (Radiography testing) rt and (visual inspection) of 9 welded plate

OPTIMIZATION AND TESTING RESULTS.

To determine the optimal parametric conditions for the SMAW (Shielded Metal Arc Welding) process, multi-objective optimization was conducted using Grey Relational Analysis (GRA). In this study, the "smaller the better" objective function was chosen for hardness, impact, and tensile properties. The steps of the Grey Relational Analysis are as follows:

Step 1: Normalization of response variables in the range 0 to 1.

Step 2: Objective functions accepted for response variables –

a) For hardness, impact and tensile –

$$Y_1^*(k) = \frac{\max Y_i^0(k) - Y_i^0(k)}{maxY_i^0(k) - minY_1^0(k)}$$

Where $Y_i^0(k)$ is the collected in experimentation and $Y_1^*(k)$ is the sequence afterward the normalization step.

Step 3: Grey relational coefficient (GRC) estimation –

GRC, $\in (k) = \frac{\Delta_{min} + \varphi\, \Delta_{mox}}{\Delta_{0i}(k) + \varphi\, \Delta_{mox}}$

Where Δ_{0i} = deviation sequence and $\Delta_{0i} = |Y_0^*(k) - Y_1^*(k)|$, $\varphi = 0.5$ is unique coefficient.

Step 4: Grey relational grade (GRG) calculation

GRG, $\alpha_j = \frac{1}{N} \sum_{i=1}^{N} w_k \in (k)$

Where w_k = 1

Step 5: Rank calculation - The optimal variables and their respective level are identified centered on the higher value of GRG

Table 4. Process Parameters Values with Respect to Their Output Responses, Normalised Value, GRG & Rank.

S N.	Exp No	Process parameters			Output response			Normalize value			GRG	Rank
		Current (Amp)	Preheat Temp (0C)	Interpass Temp (0C)	HWZ(BHN)	IWZ(J)	UTS(MPA)	HWZ	IWZ	UTS		
1	1A	100	250	100	51	6	385.08	0.4	1	0.3137	0.625	4
2	2A	100	300	200	49.66	8	394.59	0.6667	0.75	0.4494	0.580	5
3	3A	100	350	300	53	10	428.28	0	0.5	0.9305	0.571	6
4	4A	110	250	200	48.33	8	433.15	0.9333	0.75	1	0.850	1
5	5A	110	300	300	49	10	417.95	0.8	0.5	0.7831	0.637	3
6	6A	110	350	100	48.33	12	363.10	0.9333	0.25	0	0.539	7
7	7A	120	250	300	49.66	12	393.18	0.6667	0.25	0.4294	0.489	8
8	8A	120	300	100	48	14	416.30	1	0	0.7595	0.669	2
9	9A	120	350	200	50.33	12	392.75	0.5333	0.25	0.4232	0.461	9

ISSN: 2321-2810 (Online), ISSN: 2321-8525 (Print)

Table 5. Process Parameter with Their Results Of DPT, MPT, RT And Visual Inspection Of 9 Welded Plates

S No	**Plate No.**	**Current (Amp)**	**Preheat Temp (^{0}C)**	**Interpass Temp (^{0}C)**	**DPT**		**MPT**		**RT**	**Visual**	**Remarks**
					Front Plate	***Back Plate***	***Front Plate***	***Back Plate***	***Seg AB***	***Front & Back***	
1	1A	100	250	100	NSD	NSD	NSD	NSD	Porosity	NSD	Accepted
2	2A	100	300	200	NSD	Porosity	NSD	NSD	Porosity	NSD	Accepted
3	3A	100	350	300	NSD	NSD	NSD	NSD	Porosity	NSD	Accepted
4	4A	110	250	200	NSD	NSD	NSD	NSD	Porosity	NSD	Accepted
5	5A	110	300	300	NSD	NSD	NSD	NSD	Porosity	NSD	Accepted
6	6A	110	350	100	NSD	Undercut	NSD	Linear Indications	Porosity	NSD	Repair
7	7A	120	250	300	NSD	NSD	NSD	NSD	Porosity	NSD	Accepted
8	8A	120	300	100	NSD	Porosity	NSD	NSD	Porosity	NSD	Accepted
9	9A	120	350	200	NSD	NSD	NSD	NSD	Porosity	NSD	Accepted

Table 4 represent the input process parameters values with their respective output responses, normalised value, GRG and Rank. The Table 5 tells the input process variable with the results of non-destructive testing results.

Level	A	B	C
1	0.5921	0.6548	0.6112
2	0.6754	0.6290	0.6303
3	0.5397	0.5234	0.5656
Delta	0.1357	0.1314	0.0647
Rank	1	2	3

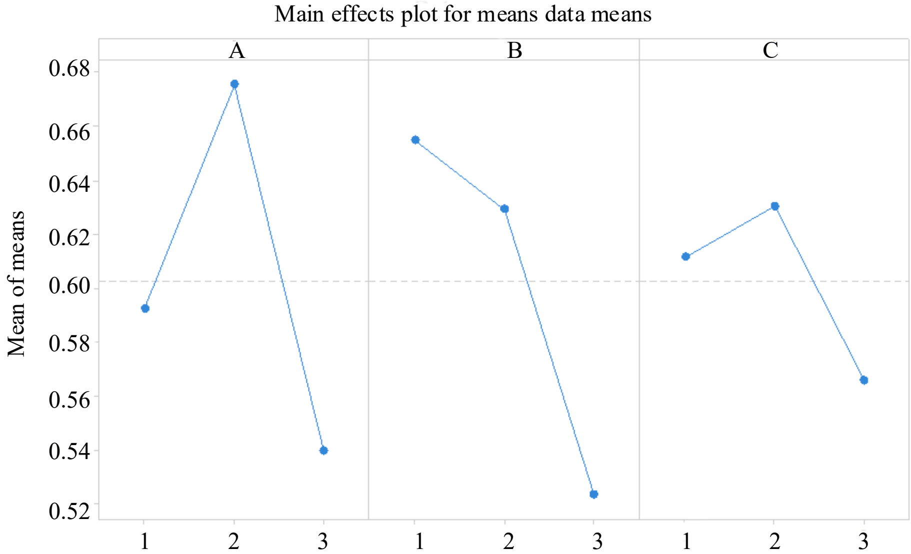

Figure 8. Main Effect Plot for A -1600 Electrodes.

The Figure 8 articulates the main effects plot highlights the impact of current, preheat, and interpass temperatures on the response variable. Current (110 A) shows the highest influence, while preheat (250°C) yields optimal results despite a negative trend. Interpass temperature (200°C) performs best, emphasizing current as the most significant parameter for A-1600.

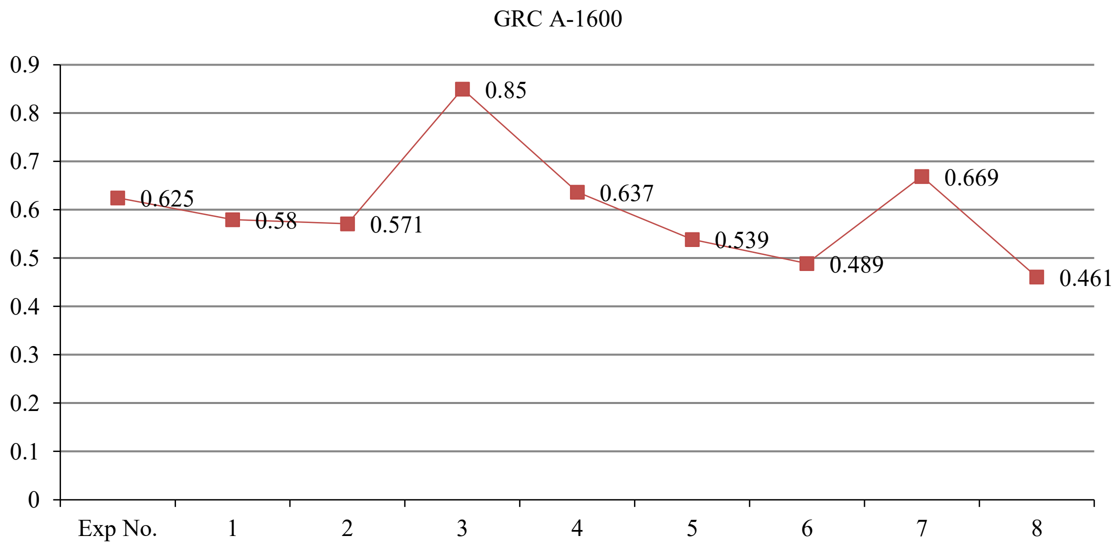

Figure 9. GRC Of A -1600 Electrode.

The Figure 9 shows the "GRC A-1600" graph displays the Grey Relational Coefficients (GRC) for the A-1600 electrode across eight experimental runs, reflecting the correlation between input conditions and desired output parameters. Experiment 3 achieves the highest GRC value of 0.85, indicating optimal welding characteristics. In contrast, experiment 8 shows the lowest GRC of 0.461, suggesting less effective parameter settings. A minor improvement is observed at experiment 7 (0.669). These variations demonstrate the significant influence of parameter combinations on electrode performance. The high GRC at experiment 3 highlights potential optimal conditions, offering valuable insights for achieving superior weld quality with the A-1600 electrode.

The Table 6 show response values according to GRG for A- 1600 electrode by considering the input parameters with their respective levels (1,2,3) and give the delta value for specific input variable. For A-1600 electrode the highest delta value occurred at current, means current was the influential parameter of this specified outcome.

The Table 7 defined the confirmation test performed on A-1600 electrode as per the L9 OA by diverse input and output parameters. The Initial settings then forecast and after that experimentation were done and output is achieved. The result shows that 0.072 improved GRG was achieved for A electrode.

RESULT AND DISCUSSION

This expresses the relationship between input and output parameters individually for A-1600 electrode by using 9 welded plates. The figure 10 reflects the relationship between input variable (Current) vs Output variable (Hardness).

Table 6. Response Values According to GRG For A-1600 Electrode.

Input variables	*Level 1*	*Level 2*	*Level 3*	Δ	*Rank*
Current	0.5921	0.6754	0.5397	0.1357	1
Preheat T	0.6548	0.629	0.5234	0.1314	2
Interpass T	0.6112	0.6303	0.5656	0.0647	3

Table 7. Confirmation Test For A-1600 Electrode.

	Initial setting	*Forecast*	*Experiential*
Level	$A_1B_1C_1$	$A_1B_2C_1$	$A_1B_2C_1$
Current	3.21		3.15
Preheat T	72.3		71.9
Interpass T	0.39		0.89
GRG	0.651	0.8049	0.723
Improved GRG	0.072		

Figure 10. Current Vs hardness of A 1600 electrodes.

The graph shows the relationship between current (100-120 A) and hardness (45-54 BHN) for plates welded with a 1600-grade electrode. Hardness peaks at 53 BHN at 100 A before dropping to 48.33 BHN. At 110 A, hardness shows minor fluctuations (49-48.33 BHN). Increasing to 120 A, hardness decreases to 48 BHN before rising to 50.33 BHN. The results highlight an optimal current (around 100 A) for maximum hardness, with non-linear effects beyond this point.

The Figure 11 expresses the line graph depicts the effect of current (100-120 A) on the impact strength of welds using an A1600 electrode and SMAW method. Impact strength starts at 6 units at 100 A, rising to 10 units and fluctuating between 8 and 14 units as current increases. The highest strength of 14 units occurs at 120 A, followed by a slight drop to 12 units. The trend shows a general increase in impact strength with rising current.

The Figure 12 illustrate the line graph shows the relationship between current (100-120 A) and tensile strength in welds using an A1600 electrode with the SMAW method. Tensile strength peaks at 433.15 MPa at 100 A before decreasing to 417.95 MPa at 110 A and dropping further to 363.1 MPa. It then rises to 416.3 MPa at 120 A before stabilizing near 392.75 MPa. The trend indicates optimal tensile strength around 100 A, with diminishing properties at higher currents.

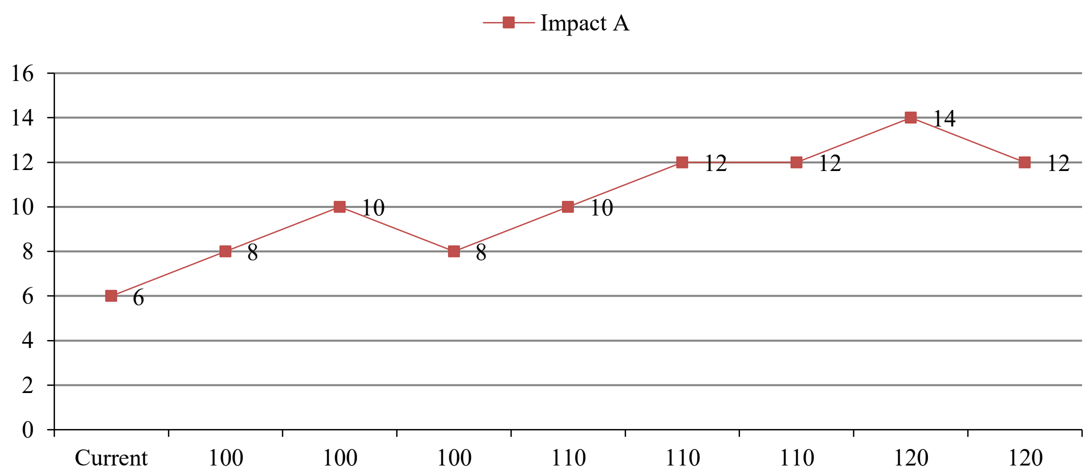

Figure 11. Current Vs Impact of A 1600 Electrodes.

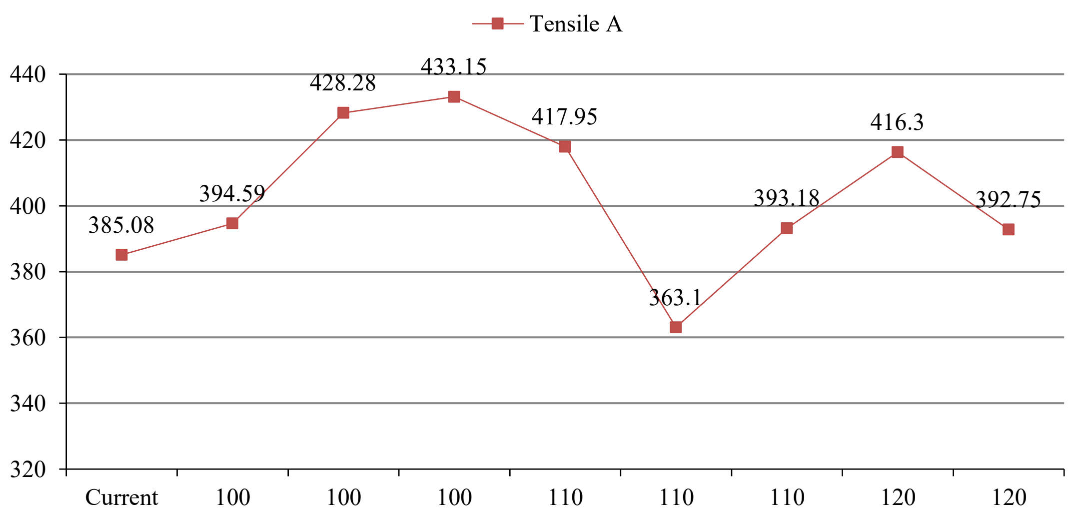

Figure 12. Current Vs tensile strength of A 1600 electrodes.

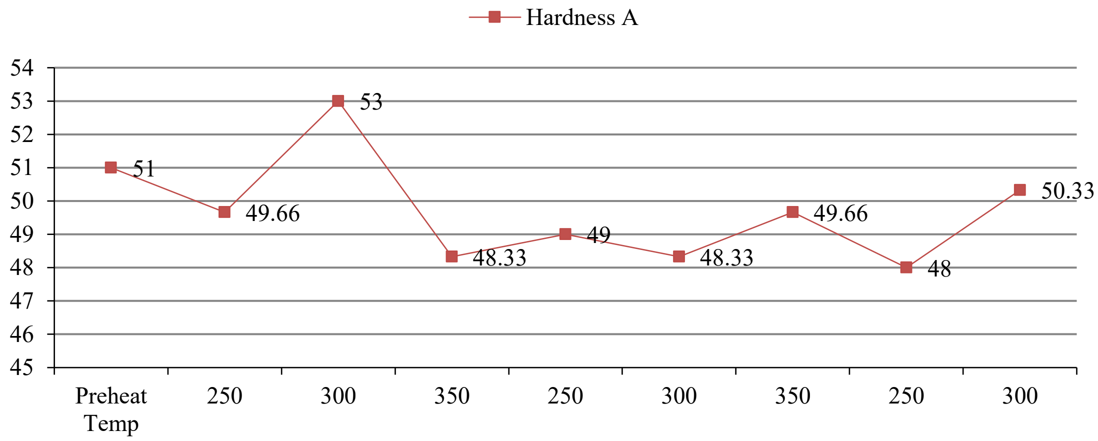

Figure 13. Preheat temperature Vs hardness of A 1600 electrodes.

The Figure 13 represent the graph shows the association of input parameter (Pre heat Temperature) of three different levels at 250,300 and 350 ^{0}C with hardness (BHN) for 9 experiments with A&B electrodes. The electrode A-1600 shows The hardness generally increases with an increase in preheat temperature, peaking at 350°C, that higher preheat temperatures had enhance the hardness of Electrode A, potentially due to improved thermal diffusion and better grain structure formation., The Electrode A exhibited a significant increase in hardness with higher preheat temperatures.

The Figure 14 states the line graph shows the effect of preheat temperature (250°C, 300°C, and 350°C) on hardness (BHN) for a welded plate using A1600 electrodes and the SMAW method. Hardness starts at 51 BHN at 250°C, drops to 49.66 at 300°C, and peaks at 53 BHN at 350°C before falling to 48.33. Repeated cycles show fluctuations between 48 and 50.33 BHN. The trend highlights the importance of precise preheat temperature control for consistent hardness results.

The Figure 15 conveys the connection among the input parameter (Pre heat Temperature) with output parameter (Tensile Strength MPa). The tensile strength generally peaks at 300°C, with a slight decrease at 350°C. This suggests that there is an optimal preheat temperature (around 300°C) for achieving the highest tensile strength for Electrode A. The higher tensile strength at 300°C could be attributed to optimal thermal diffusion and grain structure formation, whereas the decrease at 350°C might be due to overheating effects or microstructural degradation. The Electrode A exhibited its highest tensile strength at 300°C.

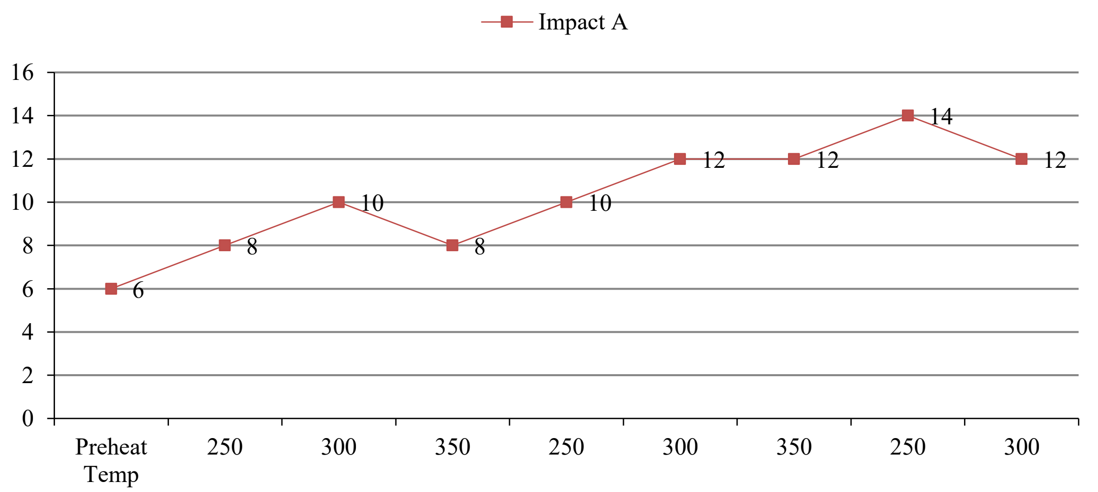

Figure 14. Preheat temperature vs impact of a 1600 electrodes.

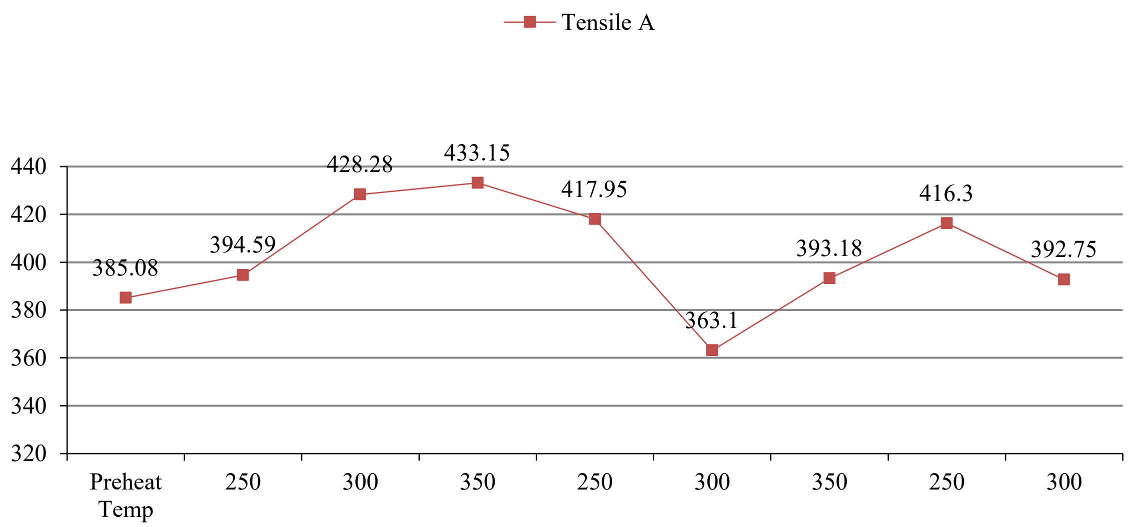

Figure 15. Preheat temperature vs tensile of A 1600 electrodes.

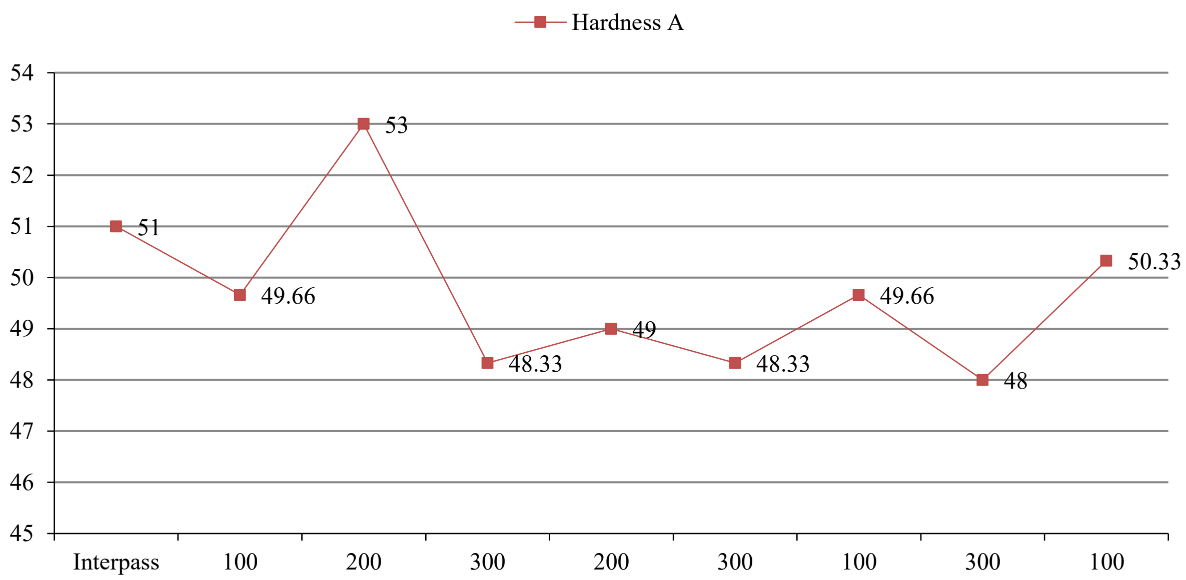

Figure 16. Interpass temperature vs hardness of welded plate of A 1600 electrodes.

The Figure 16 reveals relation between input parameter (Interpass temperature 100, 200, 300^0 C) with output parameter (Hardness BHN). The hardness generally increases with an increase in interpass temperature, peaking at 300°C. This suggests that higher interpass temperatures may enhance the hardness of Electrode A, potentially due to improved thermal diffusion and better grain structure formation. The maximum hardness achieved at 300°C was 53 BHN. Electrode A exhibited a significant increase in hardness with higher Interpass temperatures.

The Figure 17 discloses the outline between input parameter (Interpass temperature 100,200, 300^0 C) with output parameter (Impact Strength). The impact strength increases with an increase in interpass temperature, peaking at 300°C. This suggests that higher interpass temperatures may enhance the impact strength of Electrode A, potentially due to better thermal diffusion and improved microstructural properties. The highest average impact strength for Electrode A is observed at 100°C, but individual readings at 300°C also show high impact values, indicating variability in response to Interpass temperature changes.

Journal of Polymer & Composites
Volume 13, Special Issue 2
ISSN: 2321-2810 (Online), ISSN: 2321-8525 (Print)

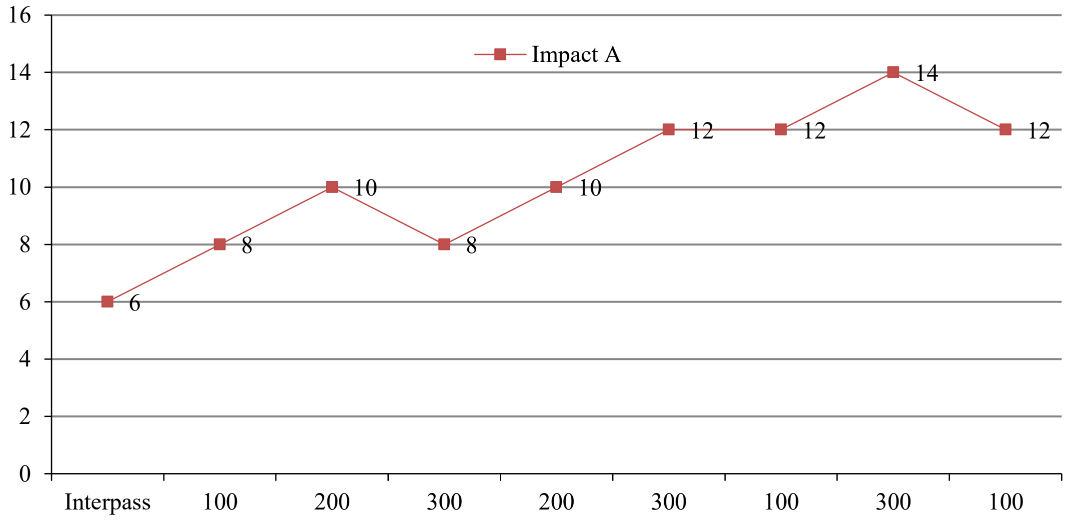

Figure 17. Interpass temperature vs impact of A 1600 electrodes.

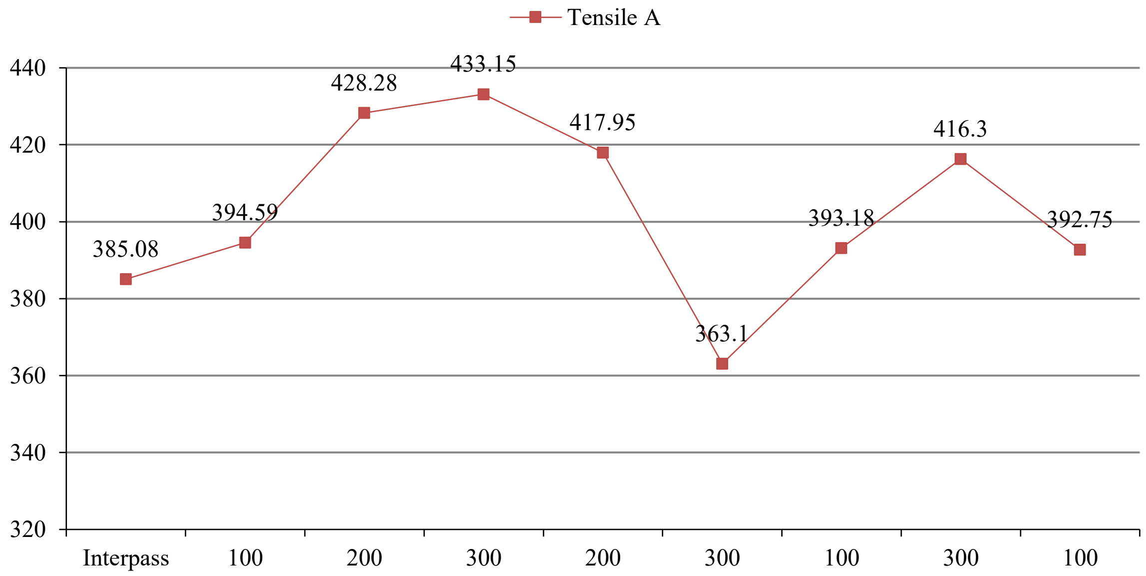

Figure 18. Interpass temperature vs tensile of A 1600 & B 850 electrodes.

The Figure 18 displays the relationship between interpass temperature and tensile strength (MPa) for Electrode A. Tensile strength increases with higher interpass temperatures, peaking at 300°C with an average of 413.14 MPa. This improvement may result from enhanced thermal diffusion and refined grain structure formation. The trend highlights that Electrode A achieves its highest tensile strength at 300°C, demonstrating a significant correlation between increased interpass temperature and improved tensile properties.

DPT (Dye Penetration Test)

The front and back plates were subjected to DPT to identify the surface defects such as porosity and undercut. The Outcomes shown that plates welded at higher currents (110-120 Amps) and increased interpass temperatures (200-300°C) exhibited fewer defects, while porosity and undercut were more frequent at lower preheat temperatures and lower interpass temperatures. This highlights the important part of optimized welding parameters in minimizing surface defects during welding processes by using A electrodes.

MPI (Magnetic Particle Inspection)

The front and back 9 welded plates were examined for surface discontinuities. The MPI results revealed that most plates showed no significant defects, denoted as NSD. However, linear indications were observed in two instances: on the back plates of 6A (110 Amps, 350°C preheat, 100°C Interpass). These findings suggest that certain combinations of welding parameters may lead to increased weakness to linear defects. The study emphasizes the importance of optimizing welding conditions to minimize surface irregularities detected by MPI.

RT (Radiography Test)

The RT marks showed that porosity was the most common flaw, observed across multiple plates irrespective of the specific parameter settings. However, precise defects such as slag inclusion, cluster porosity, and burn-through were also detected, mostly in plates with higher current and lower interpass temperatures. All the 9 Plates shows the porosityin the Testing. These findings highlight the critical role of optimizing welding factors to minimize internal defects, as detected by RT, and ensure the mechanical integrity of welded joints.

Visual Inspection

The effects presented that the majority of the plates, across all parameter settings, revealed no significant defects (NSD) and were considered as acceptable. However, two plates required repairs: plate 6A (110 Amps, 350°C preheat, 100°C interpass). These findings suggest that while most welding parameters resulted in acceptable surface quality, specific combinations may increase the possibility of repair. This study stresses the importance of visual inspection in ensuring the quality of welded joints and highlights the necessity for careful control of welding parameters to reduce defects.

CONCLUSION

The relationship between input parameters (Current in Ampere, Preheat Temperature in ^{O}C and Interpass Temperature in ^{O}C) with output parameters i.e. Mechanical properties (Hardness in BHN, Impact strength and Tensile strength in MPa) by A- 1600 Electrode by considering the L9 orthogonal array with three different level of input parameter for the application of reinforced composites and Thermoplastics material having the high strength applications. The outcome of this paper stated below

1. For considering the electrode A-1600, the Experiment number 4 gives the best result as per the optimization technique Grey Relational Analysis.
2. The Experiment 4 for the electrode A-1600 was current at 110ampere , pre heat at 250 ^{0} C and Interpass temperature at 200 ^{0} C for input parameters gives the output parameters as Hardness at 48.33 BHN, Impact at 8 and tensile strength at 433.15 MPa at welded zone. The current is the most influential input parameter for Electrode A-1600
3. The other testing like visual inspection by experts , DPT (Dye Penetration Test) , MPI (Magnetic Particle Inspection) , and RT (Radiography Testing) also done for 09 welded plate.
4. The impact of input parameter current in ampere on hardness as Higher current generally correlates with increased mechanical properties (hardness, impact resistance, tensile strength) for A-1600 Electrode, that higher welding currents lead to stronger welds and improved material properties.
5. The impact of preheat temperature on Increasing preheat temperature generally enhances mechanical properties, particularly hardness and tensile strength, for electrodes A-1600, Higher preheat temperatures likely reduce residual stresses and improve material flow during welding, contributing to improved mechanical properties.
6. The impact of Interpass temperature on Varied effects on mechanical properties were observed with changes in interpass temperature, Optimal Interpass temperatures appear to vary depending on the specific mechanical property being considered (e.g., impact resistance may benefit from different temperatures than hardness or tensile strength).

REFERENCES

1. Ahmad Naufal Rizki Aini, Tara Lydwina, Asep Ridwan Setiawan, et al. Assessing the Consequences of Repetitive Repair Welding in Shielded Metal Arc Welding (SMAW) on Material Properties in API 5L Grade B PSL 2 Welded Pipelines. Transactions of the Indian Institute of Metals- March 2024-04-21.
2. Khan, M.S., Abas, M., Qayyum, Z. et al. Effect of root pass removal procedures on mechanical and microstructural properties of shielded metal arc welded joints. Int J Adv Manuf Technol (2024). https://doi.org/10.1007/s00170-024-13591-y.
3. Darmawan, A. S., Anggono, A. D., Yulianto, A., et al. Effect of Shielded Metal Arc Welding on Microstructure, Hardness, and Tensile Strength of Nodular Cast Iron. In 6th International Conference on Advanced Materials Science. 6th International Conference on Advanced Materials Science. Trans Tech Publications Ltd. https://doi.org/10.4028/p-2gxsxr.
4. Vijayakumar, S., Arunkumar, A., Pradeep, A., et al. (2024). Optimization of process variables for shielded metal arc welding dissimilar mild steel and medium carbon steel joints. Journal of Adhesion Science and Technology, 38(2), 185–202. https://doi.org/10.1080/01694243.2023.2227461.
5. Sirohi S, Kumar N, Kumar A. Metallurgical characterization and high-temperature tensile failure of Inconel 617 alloy welded by GTAW and SMAW—a comparative study. Proceedings of the Institution of Mechanical Engineers, Part L: Journal of Materials: Design and Applications. 2023;237(9):2046-2067. doi:10.1177/14644207231171266.
6. Sirohi, S.; Pandey, S.M.; Świerczyńska, A.; et al. Microstructure and Mechanical Properties of Combined GTAW and SMAW Dissimilar Welded Joints between Inconel 718 and 304L Austenitic Stainless Steel. Metals 2023, 13, 14. https://doi.org/10.3390/met13010014.
7. Qazi, M.I.; Akhtar, R.; Abas, M.; et al. An Integrated Approach of GRA Coupled with Principal Component Analysis for Multi-Optimization of Shielded Metal Arc Welding (SMAW) Process. Materials 2020, 13, 3457. https://doi.org/10.3390/ma13163457.
8. J.P. Lee M.H. Park, D.H. Kim ,et al "An experimental study on optimizing for tandem gas metal arc welding process" JAMME, 68, pp 72-79, 2015.
9. Chuaiphan W, Srijaroenpramong L, "Optimization of gas tungsten arc welding parameters for the dissimilar welding between AISI 304 and AISI 201 stainless steels", Elsevier Defence Technology, pp1-6, 2018.
10. Seyed Mostafa Mirhedayatian , Seyed Ebrahim Vahdat , Mostafa Jafarian Jelodar , et al, "Welding process selection for repairing nodular cast iron engine block by integrated fuzzy data envelopment analysis and TOPSIS approaches", Materials and Design 43, pp 272–282, 2013.
11. M. Pouranvari, "On the weldability of grey cast iron using nickel based filler metal", Materials and Design 31, pp 3253–3258, 2010
12. Alireza Sadeghi, Ahmad Moloodi, Masoud Golestanipour, et al, "An investigation of abrasive wear and corrosion behavior of surface repair of gray cast iron by SMAW", j m a t e r r e s t e c h n o l .6(1), pp 90–95, 2017.
13. Mohsen Askari , G Paykani, MehrdadShayan, et al, "Weldability of Ferritic Ductile Cast Iron Using Full Factorial Design of Experiment", Journal Of Iron And Steel Research, International, 2 1 (2), pp 2 5 2 - 2 6 2014.
14. Olamilekan Oloyede, Robert F. Cochrane, Andrew M. Mullis, "Effect of rapid solidification on the microstructure and microhardnessof BS1452 grade 250 hypoeutectic grey cast iron", Journal of Alloys and Compounds , pp 1-4, 2016.
15. N. Ghosh , Pradip Kumar Pal, Goutam Nandi, "GMAW dissimilar welding of AISI 409 ferritic stainless steel to AISI 316L austenitic stainless steel by usingAISI 308 filler wire", Elsevier ,Eng. Sci. Tech. Int. J. ,pp 1-8, 2017.
16. V. Singh , M. Chandrasekaran & S. Samanta : Study on the influence of heat input on mechanical property and microstructure of weld in GMAW of AISI 201LN stainless steel, Advances in Materials and Processing Technologies, (2020).

17. E.M. El-Banna , M.S. Nageda , M.M. Abo El-Saadat , “Study of restoration by welding of pearlitic ductile cast iron”, Materials Letters 42, pp 311–320,2000.
18. E.M. El-Banna, “Effect of preheat on welding of ductile cast iron, Materials Letters 41, pp 20–26, 1999
19. Ahire P.G., Patil U.S., Kadam M.S., “Genetic Algorithm Based Optimisation of the Process Parameter for MMAW of Dissimilar metal joint”, Procedia Manufacturing 20 (2018) 106-112.
20. Ghosh N.,Rudrapati R., Pal P.K.,Nandi G., “Parametric Optimization of GMAW Process by using Taguchi method on Ferritic Stainless Steel AISI409”Materal Today Proceedings 4 (2017) 2213-2221.
21. Sayed A.R., Gupta R., Barai R.,“Experimental investigation of C45 (AISI 1045) weldments using SMAW and GMAW ” AIP Conference Proceedings 2148, 03004.
22. Muhammad Saad Afzal ,Optimization of process parameters for shielded metal arc welding for ASTM A 572 grade 50 - Journal of Engineering Research-11 Jan 2024.
23. Erdal Karadeniz , Ugur Ozsarac , Ceyhan Yildiz, “The effect of process parameters on penetration in gas metal arc welding processes”, Materials and Design 28 , pp 649–656, 2007.
24. Shekhar Srivastava, R.K. Garg, “Process parameter optimization of gas metal arc welding on IS:2062mild steel using response surface methodology”, Journal of Manufacturing Processes 25, 296–305, 2017.
25. Srinivasa Reddy Vempati, K.Brahma Raju, K.Venkata Subbaiah, “Optimization of Welding Parameters of Ti 6al 4v Cruciform shape Weld joint to Improve Weld Strength Based on Taguchi Method”, Materials Today: Proceedings 5 , pp 4948–4957, 2018.
26. P.K. Palani, N. Murugan, “Optimization of weld bead geometry for stainless steel claddings deposited by FCAW”, Journal of Materials Processing Technology 190 , pp 291–299, 2007.
27. Balaram Naik, A. Chennakeshava Reddy, “Optimization of Tensile Strength in TIG Welding Using Taguchi Method and Analysis of Variance (ANOVA)”, Thermal Science and Engineering Progress, pp 1-26, 2018.
28. Sudhir Kumar, Rajender Singh, “Optimization of Process Parameters of Metal Inert Gas Welding with Preheatingon AISI 1018 Mild Steel using grey based Taguchi Method”, Measurement, pp 1-19, 2019.

